ACS Catalysis

Letter

pubs.acs.org/acscatalysis

Mo_2C Nanoparticles Decorated Graphitic Carbon Sheets: Biopolymer-Derived Solid-State Synthesis and Application as an Efficient Electrocatalyst for Hydrogen Generation

Wei Cui,[†,‡] Ningyan Cheng,[†,‡] Qian Liu,[†] Chenjiao Ge,[†] Abdullah M. Asiri,[§,∥] and Xuping Sun*[,†,§,∥]

[†]State Key Lab of Electroanalytical Chemistry, Changchun Institute of Applied Chemistry, Chinese Academy of Sciences, 5625 Renmin Street, Changchun 130022, Jilin China

[‡]Graduate School of the Chinese Academy of Sciences, Beijing 100039, China

[§]Chemistry Department, Faculty of Science and [∥]Center of Excellence for Advanced Materials Research, King Abdulaziz University, P.O. Box 80203, Jeddah 21589, Saudi Arabia

Supporting Information

ABSTRACT: The present work reports on the preparation of Mo_2C nanoparticles decorated graphitic carbon sheets (Mo_2C/GCSs) via a biopolymer-derived solid-state reaction between $(NH_4)_6Mo_7O_{24}\cdot 4H_2O$ and sodium alginate at 900 °C under Ar. As a novel hydrogen evolution reaction electrocatalytst, the Mo_2C/GCSs hybrids exhibit high activity in acidic solutions with an onset potential of 120 mV, a Tafel slope of 62.6 mV dec^{-1}, and an exchange current density of 12.5×10^{-3} mA cm^{-2}. Moreover, such Mo_2C/GCSs catalysts also show excellent durability during long-term 3000 cycles.

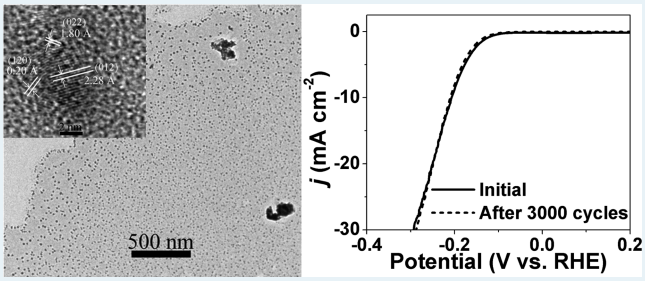

KEYWORDS: *molybdenum carbide nanoparticles, graphitic carbon sheets, biopolymer, electrocatalysts, hydrogen generation*

Hydrogen is regarded as a real alternative to fossil fuels owing to its high-energy but carbon-free content.[1−5] Realization of the hydrogen economy has led to the need for efficient and sustainable methods of generation of hydrogen. One attractive technology is direct electrochemical water splitting.[6−10] Yet in the process of hydrogen evolution reaction (HER), an advanced catalyst is required to decrease the overpotential (η) to obtain high efficiency.[11,12] To date, the most efficient elctrocatalyst for HER is Pt, which is active at a nearly zero overpotential.[13−15] Whereas, its high cost seriously limits its large-scale application. Therefore, to find less expensive and highly active substitutes has aroused intense research interest.[4,16,17]

Molybdenum compounds, such as MoS_2, MoB, and MoN, are proved to be replacements for the Pt catalyst due to their low costs and remarkable catalytic properties for HER.[18−23] Another molybdenum compound Mo_2C has been reported as a good candidate for replacing Pt, but it also shows highly effective electrocatalytic properties for HER in both acidic and basic conditions.[21,24] Recently, various carbon-supported Mo_2C nanostructures have been designed. The strong conjugation between the anchored Mo_2C particles and carbon supports inhibits the aggregation of Mo_2C nanoparticles, resulting in highly reactive sites on the surfaces. This thus favors a low overpotential, a small Tafel slope, a large exchange current density, and a reduction in charge-transfer resistance, which are all required for a good HER electrocatalyst.[25] So far, a series of carbon materials, including carbon black, carbon nanotubes, and reduced graphene oxide, have been used for supporting Mo_2C particles because of their large surface area, superior electroconductivity, and stability.[26,27]

Sodium alginate (ALG), a natural polysaccharide product extracted from brown seaweed growing in cold water regions, exists in nature widely, which implies its feasible availability and widespread application.[28] In this study, utilizing ALG as a low-cost environmentally friendly carbon source, we prepared Mo_2C nanoparticles decorated graphitic carbon sheets (Mo_2C/GCSs) via a one-step solid-state reaction between $(NH_4)_6Mo_7O_{24}\cdot 4H_2O$ and ALG for the first time. Mo_2C/GCSs were then proved to be highly active electrocatalysts for HER in 0.5 M H_2SO_4 with a low onset overpotential (120 mV), a small Tafel slope (62.6 mV dec^{-1}), a high exchange current density (12.5×10^{-3} mA cm^{-2}), and good elctroconductivity. Moreover, the Mo_2C/GCSs catalysts also show excellent long-term electrochemical stability over 3000 cycles in acidic solutions. Lastly, we explored the HER activity of catalysts formed by same precursors with different mass ratios.

Mo_2C/GCSs and GCSs were obtained from the solid-state reaction at 900 °C under Ar flow (see Supporting Information for preparation details). Graphitic structures in the products can be monitored by Raman spectroscopy. Figure 1a shows the Raman spectra of Mo_2C/GCSs and GCSs. Two expected peaks

Received: April 21, 2014
Revised: June 11, 2014
Published: July 8, 2014

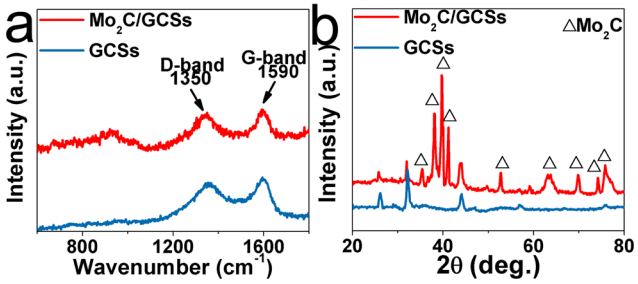

Figure 1. (a) Raman spectra and (b) XRD patterns of Mo_2C/GCSs and GCSs.

are observed at 1350 and 1590 cm^{-1}, which correspond to the D and G band of graphitic carbon, respectively. Figure 1b shows the X-ray diffraction (XRD) patterns of Mo_2C/GCSs and GCSs. Both samples show peaks at 25.9, 32.2, and 43.5°, supporting the formation of ALG-derived graphitic carbons after the pyrolysis process.[29,30] Compared with GCSs, Mo_2C/GCSs show additional diffraction peaks at 2θ = 35.3, 38.0, 39.6, 41.0, 52.6, 63.3, 70.0, 74.0, 76.0°, which can be assigned to 210, 020, 012, 120, 022, 321, 231, 420, and 014 faces of Mo_2C, respectively (JCPDS no. 77-0720).

Figure S1 shows the energy dispersive X-ray spectrum (EDS) of Mo_2C/GCSs. Peaks corresponding to C, Mo, and O elements are observed with content of 70.3%, 20.6%, and 9.11%, respectively (Si peak originates from the substrate). The observation of the O element can be attributed to the formation of O heteroatoms incorporated carbon.[31,32] Figure S2 shows the high resolution Mo 3d and C 1s X-ray photoelectron spectroscopy (XPS) spectra. The peak located at binding energy 228.4 and 231.6 eV is assigned to Mo^{2+} ($3d_{5/2}$ and $3d_{3/2}$, respectively), consistent with the carbidic phase. Other $3d_{5/2}$ and $3d_{3/2}$ binding energies 229.2 and 232.5 eV for Mo^{4+}, 231.5 and 234.5 eV for Mo^{5+}, 232.9 and 235.9 eV for Mo^{6+}. Besides, no metallic Mo is detected. The ratio of surface Mo^{2+} to the oxidation states (Mo^{5+} and Mo^{6+}) is about 0.13. Those suggest the presence of mixed oxidation states of Mo^{5+} and Mo^{6+} arising from superficial oxidation of Mo_2C due to air contact.[33,34] C 1s peaks at binding energies of 284.7 and 288.1 eV can be assigned to graphenic carbon atoms and carbon atoms bonded to oxygen atoms, respectively.[35]

Figure 2a shows the scanning electron microscopy (SEM) image of the pyrolyzed products, indicating the formation of bulk microstructures. Such microstructure was exfoliated into Mo_2C/GCSs after sonication treatment. It is of importance to mention that the absence of Mo_2C nanoparticles requires an extended sonication (700 W, 1 h) to exfoliate ALG-derived graphitic carbon; however, only 10 min of sonication at 480 W is required to achieve the exfoliation of Mo_2C/GCSs in our present study.[32] It could be attributed to the fact that these Mo_2C nanoparticles intercalated into graphitic carbon, thereby weakening the interlayer interactions between graphene layers. Figure 2b presents the low-magnification transmission electron microscopy (TEM) image of the resulting Mo_2C/GCSs, indicating the formation of large amounts of nanoparticles decorated on the thin carbon sheet. High-magnification TEM image (Figure 2c) reveals that these nanoparticles have sizes in the range of 5−23 nm. Figure 2c inset shows the corresponding particle size distribution histograms. Figure 2d shows the high-resolution TEM (HRTEM) image taken from one nanoparticle. Clear interplanar distances are observed and measured to be 1.80 and 2.28 Å, corresponding to the 022 and 012 crystal

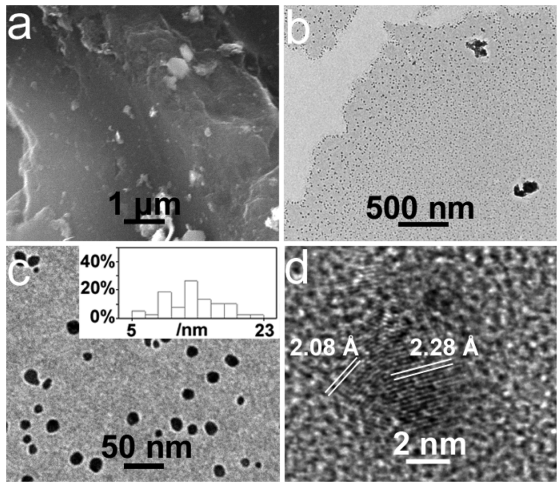

Figure 2. (a) SEM image of the pyrolyzed products, (b) low, and (c) high-magnification TEM (inset: particle size distribution histograms) and (d) HRTEM images of Mo_2C/GCSs.

planes of Mo_2C, respectively. All these observations can note that Mo_2C/GCSs have been prepared successfully through one-step solid-state reaction from $(NH_4)_6Mo_7O_{24}{\cdot}4H_2O$ and ALG. It is worth mentioning that the pyrolysis of pure sodium alginate only gives GCSs (Figure S3).

Recently, Chen et al. have developed a soybean biomass-derived Mo-based HER catalyst (MoSoy).[22] However, this catalyst is not pure Mo_2C but composed of β-Mo_2C and γ-Mo_2N phases. In addition, it requires the introduction of extra reduced graphene oxide (RGO) to obtain Mo_2C−Mo_2N composite nanoparticles decorated RGO sheet, but RGO preparation is usually time-consuming and labor-intensive.[36] Thus, our Mo_2C/GCSs catalyst is more simple with an additional advantage of facile and fast preparation.

The HER properties of the Mo_2C/GCSs and GCSs catalysts on a glassy carbon electrode (GCE) were then investigated in 0.5 M H_2SO_4 solution using a typical three-electrode system. For comparison study, commercial Mo_2C and Pt/C catalysts were also examined. Figure 3a shows the polarization curves with a sweep rate of 2 mV s^{-1}. Pt/C catalyst exhibits expected HER activity with a near zero overpotential, whereas GCSs exhibit poor HER activity. In contrast, Mo_2C/GCSs exhibit a small onset overpotential of 120 mV, which is much smaller than that of commercial Mo_2C (200 mV). In addition, for driving a current density of 10 mA cm^{-2}, Mo_2C/GCSs only need an overpotential of 200 mV. Figure S4 presents the photo of the obvious hydrogen bubbles generated on the Mo_2C/GCSs catalysts modified GCE during the initial LSV scanning. Figure 3b shows the Tafel plots for Mo_2C/GCSs, commercial Mo_2C and Pt/C. Pt/C shows an expected Tafel slope of 30 30.0 mV dec^{-1}. Mo_2C/GCSs show a Tafel slope of 62.6 mV dec^{-1}, much lower than that of commercial Mo_2C, suggesting both Mo_2C catalysts proceed via a Volmer-Heyrovsky mechanism.[19,25,37] Figure S5 presents Tafel slope and current densities histograms at potentials of 200, 250, and 300 mV (error bar represents the standard deviations of three Mo_2C/GCSs samples and three measurements for each sample).

The exchange current density (j_0) is also given, which can be obtained from Tafel plots by using extrapolation methods (see Figure S6 for details). The j_0 for Mo_2C/GCSs is determined as 12.5×10^{-3} mA cm^{-2}, which is quite a satisfactory value for noble-metal-free HER catalysts. Corrosion stability is another

dx.doi.org/10.1021/cs5005294 | ACS Catal. 2014, 4, 2658−2661

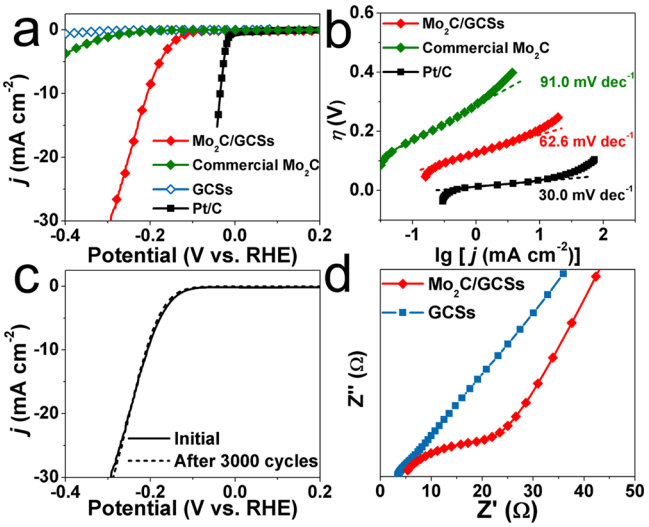

Figure 3. (a) Polarization curves of the Mo_2C/GCSs, commercial Mo_2C, GCSs, and Pt/C catalysts with a scan rate of 2 mV s^{-1} in 0.5 M H_2SO_4. (b) Tafel plots of Mo_2C/GCSs, commercial Mo_2C and Pt/C. (c) Durability test for the Mo_2C/GCSs catalyst by CV scanning for 3000 cycles in 0.5 M H_2SO_4. (d) Nyquist plots of Mo_2C/GCSs and GCSs.

important parameter for viability of a HER catalyst. We also performed the durability test of the Mo_2C/GCSs catalysts utilizing cyclic voltammetry (CV) measurements for scanning 3000 cycles in 0.5 M H_2SO_4. The observation of negligible current loss (Figure 3c) indicates that the Mo_2C/GCSs catalysts have excellent electrochemical stability in acidic electrolyte. Recently, Chen et al. found that Mo_2C nanoparticles formed in situ were anchored and inlaid into the carbon supports. We attribute the high active and stability to the coupling effect between Mo_2C nanoparticles and GCSs. The covalent binding between Mo_2C and carbon supports has been proved to facilitate electron transfer and decrease hydrogen binding energy during the HER process.[26] Graphitic carbon materials ought to achieve good electroconductivity, and we thus performed electrochemical impedance spectroscopy (EIS) measurements. Figure 3d shows the Nyquist plots of Mo_2C/GCSs and GCSs. It is seen that although GCSs shows a much smaller semicircle, the Faradaic impedance yielded by Mo_2C/GCSs is also very small, implying that Mo_2C/GCSs have good electron transfer ability. All these results demonstrate that Mo_2C/GCSs are indeed a highly efficient HER electrocatalyst. Table S1 lists HER activity parameters of various Mo-based catalysts from recent reports. All these catalysts were tested in acidic solutions. The Mo_2C/GCSs catalysts exhibit high activity for HER with a low loading of 0.36 mg cm^{-2}. It is worthwhile to mention that all carbon-supported Mo_2C catalysts exhibit a nearly 10 times larger exchange current density than bulk Mo_2C. This high j_0 can be attributed to the unique carbon sheet-supported nanostructure, which affords large amounts of active sites. In addition, integration of catalysts with carbon will enhance the electroconductivity. This verifies that carbon materials play a significant role in improving the activity of electrocatalysts.

The generated gas was confirmed by gas chromatography (GC) analysis and measured quantitatively using a calibrated pressure sensor to monitor the pressure change in the system. A galvanostatic electrolysis experiment was carried out by maintaining catalyst-loaded glassy carbon plate (1 cm^2) at a cathodic current of 10 mA for 40 min, resulting in passage of 24 C of charge. The Faradaic efficiency (FE) was calculated by comparing the amount of measured hydrogen with calculated hydrogen (assuming 100% FE), as shown in Figure S7. The FE was quantitative, and thus the current density is directly related to hydrogen generation.

We further synthesized another four samples with different mass ratios of precursors (Mo/ALG: 1:1, 1:3, 1:4, and 1:10). XRD patterns of these samples and pure GCSs are shown in Figure S8. Apparent diffraction peaks of Mo_2C are observed in each sample, suggesting the accomplishment of solid-state reactions. The HER activity of these samples was also investigated by the same measurements. Figure 4a gives the

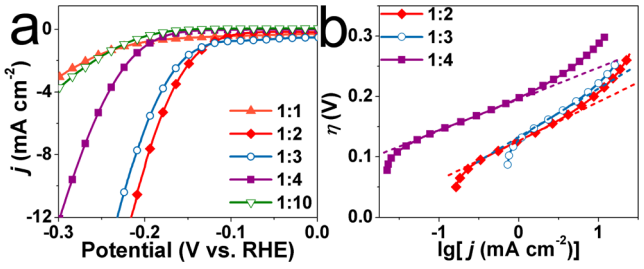

Figure 4. (a) Polarization curves and (b) Tafel plots of the catalysts derived from $(NH_4)_6Mo_7O_{24}{\cdot}4H_2O$ and ALG with different initial mass ratios (from 1:1 to 1:10).

polarization curves of these samples. Samples obtained with 1:3 and 1:4 exhibit good HER activity with slightly larger onset overpotentials (150 and 190 mV, respectively) than sample obtained with 1:2. Samples obtained with 1:1 and 1:10 exhibit relatively poor HER activity with much smaller HER current density at the same potential. Such observations suggest that a balance between the amounts of two precursors is needed for preparing a good HER electrocatalyst. Tafel slopes of samples obtained with 1:2, 1:3, and 1:4 are calculated to be 62.6, 70.6, and 58.7 mV dec^{-1}, respectively, from their Tafel plots (Figure 4b). These results clearly suggest that the mass ratio of the precursors has significant influence on HER activity of the hybrid catalysts thus prepared, and the optimized mass ratio is 1:2.

In summary, Mo_2C/GCSs have been successfully synthesized via a solid-state reaction at 900 °C under Ar using $(NH_4)_6Mo_7O_{24}{\cdot}4H_2O$ and ALG as starting materials. The alginate, which is rich in nature, can form GCSs to support Mo_2C nanoparticles after calcination. We further demonstrate the use of such Mo_2C/GCSs hybrids as a novel HER electrocatalyst with high efficiency and excellent corrosion stability in acidic media. It also suggests that the catalytic performance of the hybrids is significantly influenced by the mass ratio of the precursors. Our present study is important for the following two reasons: (1) it is the first use of ALG as a carbon source for preparing GCSs decorated with Mo_2C nanoparticles with high HER activity; (2) it provides us a general methodology for biopolymer-derived scaled-up synthesis of transition metal-based nanostructures/carbon hybrids for applications.

■ ASSOCIATED CONTENT

Supporting Information

Experimental details; EDS and XPS spectra; TEM image; photograph; the calculation of j_0; Table S1; FE determination;

dx.doi.org/10.1021/cs5005294 | ACS Catal. 2014, 4, 2658−2661

XRD patterns. This material is available free of charge via the Internet at http://pubs.acs.org.

AUTHOR INFORMATION

Corresponding Author

*E-mail: sunxp@ciac.ac.cn

Notes

The authors declare no competing financial interest.

ACKNOWLEDGMENTS

This work was supported by the National Natural Science Foundation of China (no. 21175129) and the National Basic Research Program of China (no. 2011CB935800).

REFERENCES

(1) Turner, J. A. *Science* **2004**, *305*, 972−974.
(2) Laursen, A. B.; Kegnaes, S.; Dahl, S.; Chorkendorff, I. *Energy Environ. Sci.* **2012**, *5*, 5577−5591.
(3) Kelly, T. G.; Chen, J. *Chem. Soc. Rev.* **2012**, *41*, 8021−8034.
(4) Koper, M. T. M; Bouwman, E. *Angew. Chem., Int. Ed.* **2010**, *49*, 3723−3725.
(5) Walter, M. G.; Warren, E. L.; McKone, J. R.; Boettcher, S. W.; Mi, Q.; Santori, E. A.; Lewis, N. S. *Chem. Rev.* **2010**, *110*, 6446−6473.
(6) Koper, M. T. M. *Nat. Chem.* **2013**, *5*, 255−256.
(7) Tran, P. D.; Nguyen, M.; Pramana, S. S.; Bhattacharjee, A.; Chiam, S. Y.; Fize, J.; Artero, V.; Wong, L. H.; Loo, J.; Barber, J. *Energy Environ. Sci.* **2012**, *5*, 8912−8916.
(8) Merki, D.; Vrubel, H.; Rovelli, L.; Fierro, S.; Hu, X. L. *Chem. Sci.* **2012**, *3*, 2515−2525.
(9) Stubbert, B. D.; Peters, J. C.; Gray, H. B. *J. Am. Chem. Soc.* **2011**, *133*, 18070−18073.
(10) Harman, W. H.; Peters, J. C. *J. Am. Chem. Soc.* **2012**, *134*, 5080−5082.
(11) Xu, Y.; Gao, M.; Zheng, Y.; Jiang, J.; Yu, S. *Angew. Chem., Int. Ed.* **2013**, *52*, 8546−8550.
(12) Merki, D.; Fierro, S.; Vrubel, H.; Hu, X. *Chem. Sci.* **2011**, *2*, 1262−1267.
(13) Lukowski, M. A.; Daniel, A. S.; Meng, F.; Forticaux, A.; Li, L. S.; Jin, S. *J. Am. Chem. Soc.* **2013**, *135*, 10274−10277.
(14) Jahan, M.; Liu, Z. L.; Loh, K. P. *Adv. Funct. Mater.* **2013**, *23*, 5363−5372.
(15) Kong, D. S.; Cha, J. J.; Wang, H. T.; Lee, H. R.; Cui, Y. *Energy Environ. Sci.* **2013**, *6*, 3553−3558.
(16) Greeley, J.; Jaramillo, T. F.; Bonde, J.; Chorkendorff, I. b.; Nørskov, J. K. *Nat. Mater.* **2006**, *5*, 909−913.
(17) Voiry, D.; Yamaguchi, H.; Li, J. W.; Silva, R.; Alves, D. C. B.; Fujita, T.; Chen, M. W.; Asefa, T.; Shenoy, V. B.; Eda, G.; Chhowalla, M. *Nat. Mater.* **2013**, *12*, 850−855.
(18) Jaramillo, T. F.; Jørgensen, K. P.; Bonde, J.; Nielsen, J. H.; Horch, S.; Chorkendorff, I. *Science* **2007**, *317*, 100−102.
(19) Li, Y.; Wang, H.; Xie, L.; Liang, Y.; Hong, G.; Dai, H. *J. Am. Chem. Soc.* **2011**, *133*, 7296−7299.
(20) Xie, J.; Zhang, H.; Li, S.; Wang, R.; Sun, X.; Zhou, M.; Zhou, J. F.; Lou, X.; Xie, Y. *Adv. Mater.* **2013**, *25*, 5807−5813.
(21) Vrubel, H.; Hu, X. *Angew. Chem., Int. Ed.* **2012**, *124*, 12875−12878.
(22) Chen, W.; Iyer, S.; Iyer, S.; Sasaki, K.; Wang, C. H.; Zhu, Y.; Muckerman, J. T.; Fujita, E. *Energy Environ. Sci.* **2013**, *6*, 1818−1826.
(23) Chen, W.; Sasaki, K.; Ma, C.; Frenkel, A. I.; Marinkovic, N.; Muckerman, J. T.; Zhu, Y.; Adzic, R. R. *Angew. Chem., Int. Ed.* **2012**, *51*, 6131−6135.
(24) Esposito, D. V.; Hunt, S. T.; Kimmel, Y. C.; Chen, J. *J. Am. Chem. Soc.* **2012**, *134*, 3025−3033.
(25) Chen, W. F.; Muckerman, J. T.; Fujita, E. *Chem. Commun.* **2013**, *49*, 8896−8909.
(26) Chen, W.; Wang, C.; Sasaki, K.; Marinkovic, N.; Xu, W.; Muckerman, J. T.; Zhu, Y.; Adzic, R. R. *Energy Environ. Sci.* **2013**, *6*, 943−951.
(27) Seol, M.; Youn, D. H.; Kim, J. Y.; Jang, J. W.; Choi, M.; Lee, J. S.; Yong, K. *Adv. Energy Mater.* **2013**, DOI: 10.1002/aenm.201307075.
(28) Schnepp, Z. *Angew. Chem., Int. Ed.* **2011**, *52*, 1096−1108.
(29) Atienzar, P.; Primo, A.; Lavorato, C.; Molinari, R.; Garcia, H. *Langmuir* **2013**, *29*, 6141−6146.
(30) Lavorato, C.; Primo, A.; Molinari, R.; Garcia, H. *ACS Catal.* **2014**, *4*, 497−504.
(31) Raymundo-Piñero, E.; Leroux, F.; Béguin, F. *Adv. Mater.* **2006**, *18*, 1877−1882.
(32) Latorre-Sánchez, M.; Primo, A.; Garcia, H. *Angew. Chem., Int. Ed.* **2013**, *52*, 11813−11816.
(33) Zou, J.; Xiang, M.; Hou, B.; Wu, D.; Sun, Y. *J. Nat. Gas Chem.* **2011**, *20*, 271−280.
(34) Świątowska-Mrowiecka, j.; de Diesbach, S.; Maurice, V.; Zanna, S.; Klei, L.; Briand, E.; Vickridge, I.; Marcus, P. *J. Phys. Chem. C* **2008**, *112*, 11050−11058.
(35) Okpalugo, T. I. T.; Papakonstantinou, P.; Murphy, H.; McLaughlin, J.; Brown, N. M. D. *Carbon* **2005**, *43*, 153−161.
(36) Hummers, W. S.; Offeman, R. E. *J. Am. Chem. Soc.* **1958**, *80*, 1339.
(37) Conway, B. E.; Tilak, B. V. *Electrochim. Acta* **2002**, *47*, 3571−3594.